Mechanism of Penetration of Antp(43−58) into Membrane Bilayers†

Wenyi Zhang and Steven O. Smith*

Department of Biochemistry and Cell Biology, Center for Structural Biology, Stony Brook University, Stony Brook, New York 11794-5215

Received February 23, 2005; Revised Manuscript Received May 23, 2005

ABSTRACT: Antp(43−58) is one of many peptides with basic and aromatic residues capable of crossing cell membranes efficiently in a receptor-independent manner. The basic−aromatic motif is responsible for peptide binding to the negatively charged surface of membrane bilayers. However, the mechanism of membrane penetration is unclear. We use high-resolution ^{1}H solution NMR methods to establish the location of the Antp(43−58) peptide bound to membrane bicelles composed of DMPC, DMPG, and DHPC, and compare it to the location of an Antp(43−58) variant which is not able to cross cell membranes. Two critical tryptophans are substituted with phenylalanine in this variant (W48F and W56F). Additional ^{31}P and ^{2}H NMR measurements of membrane bicelles are used to probe the changes in orientation of the lipid headgroups and the changes in the mobility or segmental order of the lipid acyl chains upon peptide binding. We find that Trp48 and Trp56 of Antp(43−58) insert into the hydrophobic core of the membrane and that this induces a change in the orientation of the negatively charged DMPG headgroups. The depth of insertion and the change in lipid orientation are concentration-dependent and argue for an electroporation-like mechanism for membrane penetration.

Clusters of basic and aromatic amino acids are often involved in the binding of peptides and proteins to cell membrane surfaces (*1*). Recently, several peptide and protein sequences with basic−aromatic motifs have been identified as being able to cross cell membranes in a receptor-independent fashion (*2, 3*). These sequences include the third helix of the Antennapedia homeodomain, the HIV TAT protein, and the HSV VP22 protein (*4*). In vitro and in vivo (*5*) studies have shown that these peptides, collectively termed Trojan peptides, can serve as vectors to deliver hydrophilic cargos ranging from polypeptides to DNA across cell membranes without inducing leakage (*6*). They are of considerable interest because of their potential for drug delivery across cell membranes (*7, 8*).

Here we investigate Antp(43−58),[1] a 16-amino acid peptide corresponding to the third helix of the Antennapedia homeodomain. The Antp(43−58) sequence (Table 1) is composed of basic and hydrophobic amino acids, including two critical tryptophans, Trp48 and Trp56. The structure of Antp(43−58) and its ability to translocate across cell membranes have been extensively studied. Importantly, when the two Trp residues in the Antp(43−58) sequence are substituted with Phe, the peptide is no longer able to cross cell membranes (*2*). We refer to the latter peptide as Antp-(43−58)-2F.

Table 1: Sequences of Antp(43−58), Antp(43−58)-2F, Arg9, and MARCKS(151−175)

RQILIWFQNRRMKWKK	Antp(43−58)
RQILIFFQNRRMKFKK	Antp(43−58)-2F
RRRRRRRRR	Arg9
KKKKKRFSFKKSFKLSGFSFKKNKK	MARCKS(151−175)

The sequence requirements for the Antp(43−58) peptide to penetrate membranes have been investigated using a wide range of designed sequence variants of Antp(43−58). Antp sequence variants generally show that a net positive charge is needed for membrane binding and that tryptophans are required for membrane penetration (*9*−*13*). Derossi and colleagues designed peptides comprised solely of arginine and tryptophan distributed on opposite faces of an α-helix (*8, 14*), and demonstrated that they were capable of transit into cells either alone or coupled with cargo. Also, enantiomeric forms of Antp(43−58) and Antp variants with inverted sequences are able to penetrate cell membranes, indicating that there is no specific receptor involved (*2, 15*).

The specific structural requirements for membrane penetration of Antp(43−58) have been studied using a wide range of biophysical methods. The Antp(43−58) peptide is helical at low peptide-to-lipid ratios and becomes less helical at high peptide-to-lipid ratios (*16, 17*). The observation of helical secondary structure has suggested that the helical amphipathic character of Antp(43−58) is needed for cell penetration (*13*). However, variants of the Antp(43−58) sequence, where one or three prolines disrupt the helical

† This work was supported by NIH−NSF instrumentation grants (S10 RR13889 and DBI-9977553) and a grant from the National Institutes of Health (GM-06965).

* To whom correspondence should be addressed: Department of Biochemistry and Cell Biology Z = 5215, Stony Brook University, Stony Brook, NY 11794-5215. Telephone: (631) 632-1210. Fax: (631) 632-8575. E-mail: steven.o.smith@sunysb.edu.

[1] Abbreviations: Antp, Antennapedia; DMPC, 1,2-dimyristoyl-*sn*-glycero-3-phosphocholine; DMPG, 1,2-dimyristoyl-*sn*-glycero-3-[phospho-*rac*-(1-glycerol)]; DHPC, 1,2-dihexanoyl-*sn*-glycero-3-phosphocholine; FACS, fluorescence-activated cell sorter; HEPES, 2-[4-(2-hydroxyethyl)-1-piperazinyl]ethanesulfonic acid; MARCKS, myristoylated alanine-rich C kinase substrate; MALDI, matrix-assisted laser desorption ionization; MAS, magic angle spinning; NOESY, nuclear Overhauser effect spectroscopy; PC, phosphocholine; SDS, sodium dodecyl sulfate; TMS, tetramethylsilane.

10.1021/bi050341v CCC: $30.25
Published on Web 07/02/2005

structure, are still able to cross cell membranes, indicating that helical secondary structure is not strictly required (*2*).

Three mechanisms are currently being considered for how Antp(43−58) peptides cross membrane bilayers. Derossi (*2*, *8*) and Prochiantz (*18*) proposed that Antp(43−58) induces the formation of inverse micelles. In the inverse micelle model, the peptide and hydrophilic cargo are captured in an aqueous compartment that moves across the membrane. In this model, the peptide remains bound to the membrane−water interface (*18*), consistent with fluorescence studies indicating that the two tryptophans in Antp(43−58) are only partially buried in membrane vesicles (*19*). Moreover, inverted micelles would not induce vesicle leakage in cell membranes, as observed (*13*). The mechanism, however, relies largely on the ability of Antp(43−58) to induce a lamellar to hexagonal phase transition of lipid membranes. ^{31}P NMR studies of Berlose et al. (*20*) have often been cited to support the view that Antp(43−58) induces a transition to hexagonal phase lipids. However, the reported ^{31}P NMR spectra of Antp(43−58) bound to membranes only exhibit resonances characteristic of isotropic and lamellar phase lipids.

The second mechanism model for how the Antp(43−58) peptide crosses membrane bilayers involves an electroporation-like mechanism (*21*). Binder and Lindblom proposed that at high peptide-to-lipid (1:20) molar ratios the asymmetric distribution of peptide (and charge) across the membrane causes a transmembrane electric field that disrupts the local bilayer structure. This model is consistent with the observation that Antp(43−58) does not induce leakage into vesicles (*13*) and is consistent with NMR data indicating that the peptide penetrates into the membrane headgroup region of the bilayer (*22*). However, this model does not explain the difference in penetration between Antp(43−58) and Antp(43−58)-2F unless the Antp(43−58) peptide is significantly more buried in membrane bilayers than Antp(43−58)-2F. NMR data in SDS micelles and membrane bicelles indicate the opposite; the N-terminus of Antp(43−58)-2F appears to be more deeply buried than that of Antp(43−58) (*22*).

The third mechanism proposed in the literature is one in which the Trojan peptides do not directly penetrate membranes, but rely on endocytic pathways (*23*). The endocytic mechanism is very likely not receptor specific on the basis of the wide range of sequences that can be internalized. Melikov and co-workers (*23*) re-evaluated the two methods typically used to show uptake of basic peptides into cells: fluorescence microscopy on fixed cells and fluorescence-activated cell sorter (FACS) analysis. They found that with two peptides, Arg9 and HIV-1 TAT, cell fixation leads to artifactual penetration of peptides into cells and that the FACS analysis is not valid unless a protease step is included. Moreover, they found that the kinetics of uptake were similar to the kinetics of endocytosis, indicating that the uptake was consistent with an endocytic mechanism (see also ref *24*). One important question with the endocytic mechanism is whether it applies equally to basic peptides, like Arg9 and TAT, and to peptides with basic−aromatic clusters. Surface binding of the strictly basic peptides may not allow the penetration of the membrane surface needed to induce the membrane curvature or distortion needed for direct permeation of the peptides through the membrane. In this regard, the size of the cargo that can be transported by Antp(43−58) appears to be limited in molecular weight (*25*, *26*), which is not the case for HIV-1 TAT (*27*).

Another mechanism for how Antp(43−58) crosses membranes, which has been largely dismissed, is one in which the peptide forms pores in membranes in a fashion similar to those of several cell permeant antimicrobial peptides (*28*−*30*). This mechanism has been ruled out on the basis of several observations (*13*, *31*). For example, conduction experiments have not been able to detect pore formation (*2*, *6*). Formation of a pore would result in vesicle leakage, which has not been observed for Antp(43−58) even at high peptide-to-lipid ratios (*13*).

The three competing mechanisms can be distinguished on the basis of (1) the location of the Antp(43−58) peptide bound to membranes, (2) the concentration dependence of membrane penetration, and (3) the ability of Antp(43−58) to locally disrupt bilayers. In this paper, we compare the location and membrane interactions of Antp(43−58) and Antp(43−58)-2F using several complementary NMR approaches. We have previously shown that high-resolution magic angle spinning (MAS) and two-dimensional (2D) nuclear Overhauser enhancement spectroscopy (NOESY) can be combined to establish the specific membrane location of aromatic amino acids on the MARCKS(151−175) peptide in multilamellar membranes (*32*). Here, we make use of ^{1}H NMR spectroscopy of the Antp peptide bound to membrane bicelles to investigate how Antp(43−58) binds and penetrates cell membranes. Membrane bicelles are small disks of membrane bilayers bordered by short chain lipids (*33*). Isotropic (nonaligned bicelles) can yield high-resolution ^{1}H spectra in an aqueous environment without MAS. On the basis of ^{1}H NOESY NMR data, we show that the Antp(43−58) peptide is able to deeply penetrate membranes to the level of the lipid acyl chains. We also have used ^{31}P NMR to investigate the orientation and mobility of the lipid headgroups in magnetically aligned bicelles, and ^{2}H NMR to investigate the effect of peptide binding on the segmental order of the lipid acyl chains. These data indicate that Antp(43−58) disrupts the local bilayer structure in a concentration-dependent manner. Taken together, the NMR data are most consistent with an electroporation-like mechanism for membrane penetration.

MATERIALS AND METHODS

Materials. 1,2-Dimyristoyl-*sn*-glycero-3-phosphocholine (DMPC), 1,2-dimyristoyl-*sn*-glycero-3-[phospho-*rac*-(1-glycerol)] (DMPG), 1,2-dihexanoyl-*sn*-glycero-3-phosphocholine (DHPC), and 1,2-dimyristoyl-D54-*sn*-glycero-3-phosphocholine (chain-deuterated DMPC) were obtained from Avanti Polar Lipids (Alabaster, AL) and used without further purification. D_2O (99.9%) was purchased from Acros Organics (Geel, Belgium). Deuterium-depleted H_2O was acquired from Cambridge Isotope Laboratory (Andover, MA).

Peptide Synthesis and Purification. Peptides corresponding to the third helix of the Antennapedia homeodomain were synthesized by solid phase FMOC chemistry. The sequences of Antp(43−58) and Antp(43−58)-2F are shown in Table 1. The synthetic peptides were purified by reverse phase HPLC (Varian Prostar) on a C4 column with an acetonitrile/

water gradient and lyophilized. The solvents contained 0.1% (w/v) trifluoroacetic acid. The purity was confirmed with MALDI mass spectrometry and HPLC.

Arg9 was synthesized by solid phase FMOC chemistry. To remove trifluoroacetic acid, the peptide was solubilized in HFIP (1,1,1,3,3,3-hexafluoro-2-propanol) and lyophilized. The peptide purity was confirmed with MALDI mass spectrometry.

Sample Preparation and Spectroscopy for High-Resolution Solid State MAS NMR of Membrane Multilayers. DMPC and DMPG lipids were codissolved in cyclohexane and lyophilized. The lyophilized powder was hydrated with 20 mM HEPES, 30 mM NaCl buffer (pH 7.0). The vesicles were subjected to 10 freeze−thaw−sonication cycles. Peptides were then added to a solution of the vesicles, and the vesicles were pelleted by ultracentrifugation at 265000*g* to form hydrated multilamellar membranes. The hydrated pellets were then transferred to the NMR rotors for MAS experiments.

Solid state ^{31}P and ^{1}H NMR experiments were performed at 360 and 700 MHz on Bruker Avance NMR spectrometers with 4.0 and 2.5 mm MAS probes, respectively. The MAS frequency was maintained at 6000 ± 2 Hz. The temperature was maintained at 30 °C. ^{1}H chemical shifts were referenced to external TMS. ^{31}P chemical shifts were referenced to external 85% H_3PO_4.

Sample Preparation and Spectroscopy for High-Resolution Solution State NMR of Membrane Bicelles. The samples containing DMPC and DMPG were prepared by first codissolving the lipids in chloroform. After the chloroform had been removed with a flow of argon gas, the lipids were redissolved in cyclohexane and lyophilized to form a fluffy powder. For deuterium NMR experiments, a portion (20%) of the protonated DMPC was substituted with chain-deuterated DMPC. DHPC was separately dissolved in cyclohexane and lyophilized overnight. The DHPC powder was hydrated with H_2O buffer or deuterium-depleted H_2O buffer (pH 7, 30 mM NaCl, 20 mM HEPES) at 30 °C, and the solution was subjected to five freeze−thaw cycles. The DHPC solution was then added to the lyophilized DMPC/DMPG powder. A final lipid concentration of 15% (w/w) was reached by diluting the sample with deuterium-depleted H_2O buffer or with H_2O buffer containing 5% D_2O. The solution was incubated at 38 °C for 20 min and then at 4 °C for 20 min. Ten cycles of incubation were repeated to form a transparent bicelle solution.

NMR experiments with isotropic and oriented bicelles were performed on a Bruker Avance NMR spectrometer at 700 MHz using a 5 mm TXI probe for ^{1}H observe experiments or a 5 mm BBO probe for ^{31}P and ^{2}H observe experiments. The ratio (or q value) of long chain to short chain lipids determines the morphology of the bicelle (*34*). Isotropic bicelles with a 1:1 ratio of long to short chain lipids ($q = 1$) were used for the ^{1}H NOESY experiments. Oriented bicelles with a 4:1 ratio of long to short chain lipids ($q = 4$) were used for ^{31}P and ^{2}H NMR experiments. For the experiments on oriented ($q = 4$) bicelles, the bicelles were oriented by heating the sample in the magnet at 45 °C for 40 min. The temperature was then maintained between 27 and 30 °C for data collection, well above the phase transition temperature of ~22 °C for the DMPC/DMPG bilayers. ^{1}H chemical shifts were referenced to external TMS. ^{31}P chemical shifts were referenced to external 85% H_3PO_4.

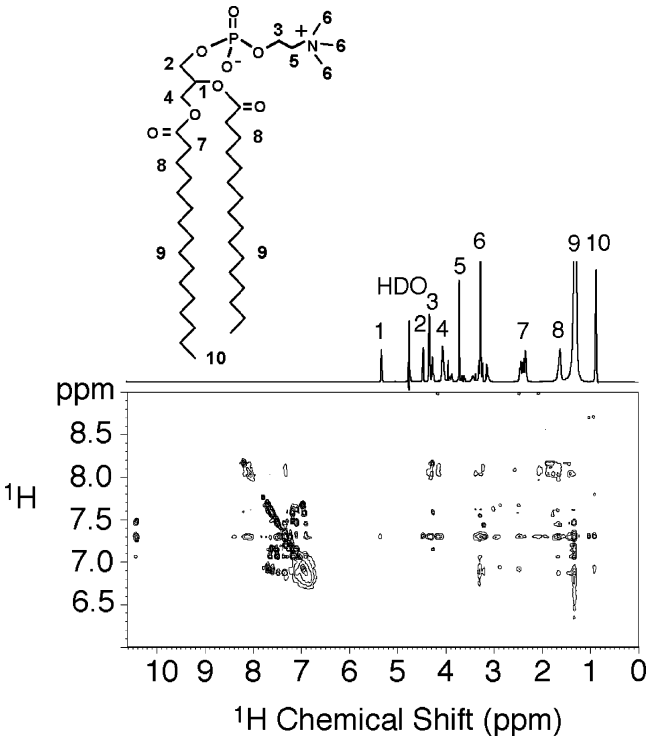

FIGURE 1: Two-dimensional high-resolution ^{1}H NOESY NMR of Antp(43−58) bound to membrane bicelles. The isotropic bicelles ($q = 1$) were made from DMPC, DMPG, and DHPC (10:3:13). The peptide:lipid ratio was 1:100, and the NOESY mixing time was 50 ms. For reference, the 1D ^{1}H spectrum of DMPC is shown along with its molecular structure. The numbering on the DMPC structure corresponds to the ^{1}H NMR assignments indicated on the 1D spectrum. ^{1}H chemical shifts were referenced to external TMS.

RESULTS AND DISCUSSION

^{1}H NOESY NMR of Antp(43−58) and Antp(43−58)-2F. The interaction of Antp(43−58) and Antp(43−58)-2F with membrane bilayers was studied using membrane bicelles (*22*). This approach has previously been used to characterize the membrane binding of basic−aromatic peptides, including the MARCKS effector domain (*35*). Membrane bicelles are relatively flat patches of bilayer membranes. The edge of the bilayer formed by the lipid acyl chains is capped by short chain lipids (e.g., DHPC in our experiments) that are roughly perpendicular in orientation to the long chain, bilayer-forming lipids. The ratio (or q value) of long chain to short chain lipids determines the morphology of the bicelle (*33*, *34*). Isotropic bicelles with a 1:1 ratio of long to short chain lipids ($q = 1$) were used for the ^{1}H NOESY experiments described in this section. Oriented bicelles with a 4:1 ratio of long to short chain lipids ($q = 4$) were used for ^{31}P and ^{2}H NMR experiments (described below).

Figure 1 presents a column from the two-dimensional NMR ^{1}H NOESY spectrum of Antp(43−58) bound to DMPC/DMPG bicelles. The intense resonances between 7 and 8 ppm correspond to diagonal resonances of the protons on the aromatic indole ring of tryptophan. The Trp aromatic resonances exhibit cross-peaks to the lipid resonances between 1 and 5 ppm. For reference, the one-dimensional (1D) spectrum of DMPC is shown at the top of the figure with a model of DMPC indicating the assignments of the acyl chain and headgroup protons (*32*). The spectrum was obtained with a NOESY mixing time of 50 ms to limit the

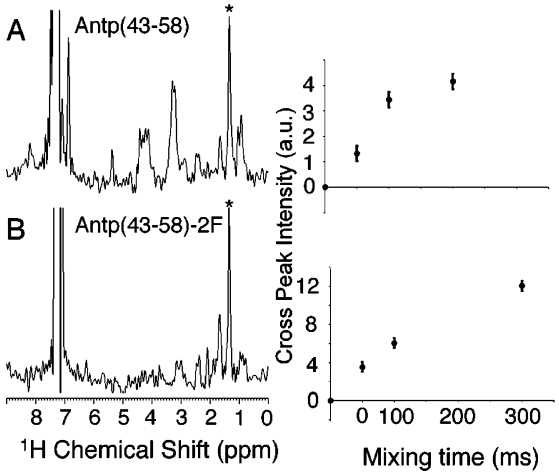

FIGURE 2: Comparison of ^{1}H NOESY spectra of Antp(43−58) and Antp(43−58)-2F. Rows are shown from the aromatic region of the 2D ^{1}H NOESY spectra of Antp(43−58) (A) and Antp(43−58)-2F (B) bound to isotropic bicelles ($q = 1$) made from DMPC, DMPG, and DHPC (10:3:13). The peptide:lipid ratio was 1:100, and the NOESY mixing time was 50 ms. The cross-peak at 1.3 ppm between the aromatic protons of the Trp or Phe rings and the methylene protons on the lipid acyl chains is marked with an asterisk. The right-hand panels show the NOE buildup curves for the 1.3 ppm cross-peak.

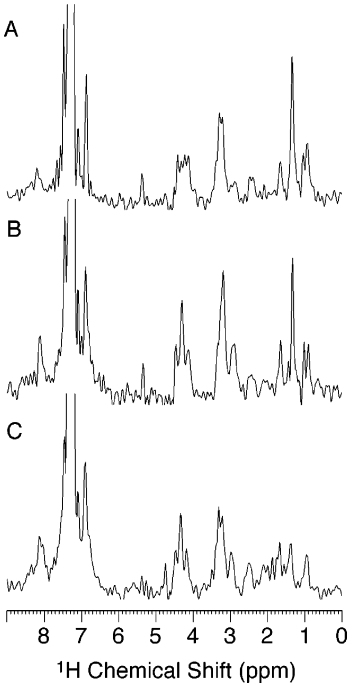

FIGURE 3: ^{1}H NOESY spectra of Antp(43−58) bound to membrane bicelles containing deuterated lipids. Rows are shown from the aromatic region of the 2D NMR ^{1}H NOESY spectra of Antp(43−58) bound to isotropic bicelles ($q = 1$) made from DMPC, DMPG, and DHPC (10:3:13). In panel A, all of the lipids are protonated. In panel B, [^{2}H]DHPC is substituted for [^{1}H]DHPC. In panel C, [^{2}H]DMPC is substituted for [^{1}H]DMPC. The NOESY mixing time was 50 ms.

effects of spin diffusion (*32*). Stronger cross-peaks are generally observed at longer (300 ms) mixing times, but the cross-peaks cannot reliably be assigned to the closest peptide−lipid contacts.

Isotropic ($q = 1$) bicelles are membrane bilayer disks estimated to be 10−20 nm in diameter (*33*, *34*). The samples of Antp(43−58) and Antp(43−58)-2F bound to bicelles are made by simply titrating the peptides into the bicelle solution. Panels A and B of Figure 2 present the rows from the aromatic region (at 7.3 and 7.2 ppm, respectively) of the 2D ^{1}H NOESY NMR spectra of the Antp(43−58) and Antp-(43−58)-2F peptides obtained using a peptide:lipid molar ratio of 1:100. In both spectra, the mixing time was 50 ms and the most intense cross-peak (marked with an asterisk) at 1.3 ppm corresponds to the methylene protons of the lipid acyl chains. The right-hand panels in Figure 2 show how the intensity of the 1.3 ppm cross-peak builds up as a function of the NOE mixing time. The rapid increase in intensity and negative curvature for the Antp(43−58) peptide is consistent with the aromatic ring protons and lipid acyl chain protons being close in space. These spectra indicate that one or more of the aromatic groups of Antp(43−58) and Antp(43−58)-2F penetrate into the hydrophobic core of the membrane.

The position of the aromatic groups can be further constrained by considering the intensity of cross-peaks with other lipid resonances. The resonances at ∼0.9 and 1.7 ppm correspond to the protons associated with the terminal methyl groups of the lipid chains and the CH_2 group closer to the acyl chain carbonyl, respectively. There are weak cross-peaks to these resonances indicating that the aromatic rings are located below the level of the acyl chain carbonyls, but above the center of the bilayer. The Antp(43−58) spectrum also contains relatively intense cross-peaks to resonances between 3 and 5 ppm, corresponding to the glycerol and choline headgroup. These cross-peaks also exhibit a rapid increase in intensity with mixing time, and the NOE buildup curves have negative curvature. The proximity of the Trp aromatic rings to both the headgroup and lipid acyl chain protons would be consistent with either a distribution of locations for the peptide or previous studies showing that Trp48 is more deeply inserted than Trp56 (*22*).

To verify that the intense cross-peak in Figure 2A is due to the methylene protons of the lipid acyl chains of DMPC (and DMPG), ^{1}H NOESY spectra of Antp(43−58) were obtained of isotropic bicelles prepared with deuterated lipids. Figure 3A presents the 1D row shown in Figure 2A at 7.3 ppm and compares it to corresponding rows obtained using chain-deuterated DHPC (Figure 3B) and chain-deuterated DMPC (Figure 3C). The spectrum in Figure 3B with [^{2}H]-DHPC looks remarkably similar to the spectrum in Figure 3A. In contrast, deuteration of DMPC results in a loss of intensity at 1.3 ppm. These data confirm the assignment of the cross-peak at 1.3 ppm as a close contact between the Trp groups of Antp(43−58) and the acyl chains of the DMPC. [The data in Figure 3 also support the choice of $q = 1$ bicelles for our measurements by confirming that the DMPC and DHPC do not form mixed-lipid micelles. It is increasingly being recognized that the morphology of bicelles changes dramatically as the q value is increased (*34*). We have found that for low values of q (e.g., $q = 0.5$), the combination of DMPC and DHPC forms mixed globular micelles rather than bicelles.]

Panels A and B of Figure 4 present the aromatic and NH rows from the Antp(43−58) peptide, respectively, obtained using a peptide/lipid molar ratio of 4:100. The 2D spectrum was obtained in H_2O. In Figure 4A, the most intense cross-peak to the aromatic diagonal resonance at 7.3 ppm corresponds to the acyl chain protons at 1.3 ppm. However, there is considerable intensity in the cross-peak at 0.9 ppm which

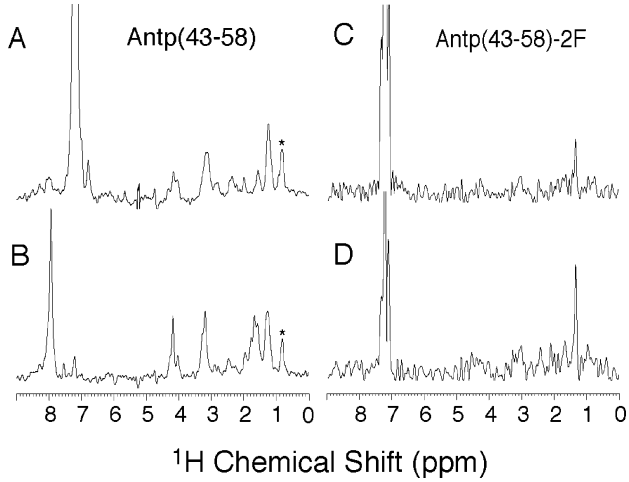

FIGURE 4: ^{1}H NOESY spectra of Antp(43−58) and Antp(43−58)-2F bound to membrane bicelles at a high peptide:lipid ratio. Rows are shown from the aromatic (A, C, and D) and NH (B) regions of the 2D NMR ^{1}H NOESY spectra of Antp(43−58) and Antp(43−58)-2F bound to isotropic bicelles (q = 1) made from DMPC, DMPG, and DHPC (10:3:13). The peptide:lipid ratio was 4:100. The NOESY mixing time was 50 ms for panels A−C and 300 ms for panel D. The cross-peak at 0.9 ppm between the aromatic (A) or NH (B) protons of the peptide and the methyl protons on the lipid acyl chains is marked with an asterisk.

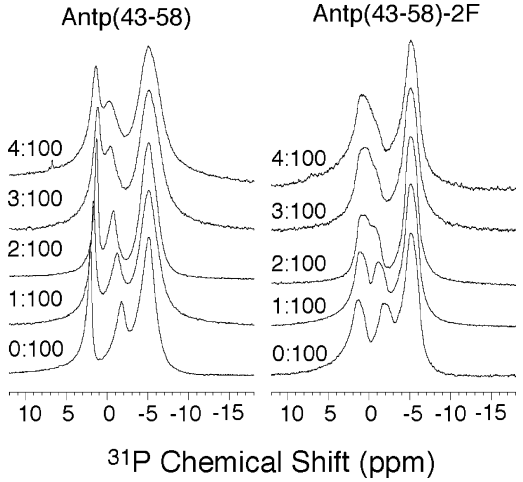

FIGURE 5: ^{31}P spectra of membrane bicelles containing Antp(43−58) (left) and Antp(43−58)-2F (right). The DMPC/DMPG/DHPC (10:3:3.25) bicelles were titrated with Antp peptide at molar ratios (peptide:lipid) from 0:100 to 4:100. The temperature was maintained at 27 °C. ^{31}P chemical shifts were referenced to external 85% H_3PO_4.

corresponds to the terminal methyl protons of the lipid chains. The higher intensity of the 0.9 ppm cross-peak relative to that of the 1.3 ppm cross-peak in Figure 4A compared to the data in Figure 2A indicates that the Antp(43−58) peptide at a higher concentration is located more deeply in the bicelle and/or causes significant membrane deformation. The intensities of the cross-peaks associated with the NH diagonal resonance at 7.9 ppm (Figure 4B) support this conclusion. The NH protons from the 16 amino acids in Antp(43−58) are not resolved. However, cross-peaks to the lipid resonances at 0.9 and 1.3 ppm indicate that several of the NH protons are deeply embedded in the bilayer. Local disruption of the membrane by binding of the Antp(43−58) peptide may allow the terminal methyl groups to bend toward the membrane surface (*36*).

Panels C and D of Figure 4 present the aromatic row (7.2 ppm) from the Antp(43−58)-2F peptide obtained using a peptide:lipid molar ratio of 4:100 and mixing times of 50 and 300 ms, respectively. The ^{1}H NOESY spectrum of Antp(43−58)-2F obtained at a peptide:lipid molar ratio of 4:100 is very similar to that obtained at a ratio of 1:100 (Figure 2B), but differs considerably from the spectrum of Antp(43−58) in Figure 4A. These data indicate that the functional difference between the Antp(43−58) and Antp(43−58)-2F peptides may be observed only at high peptide:lipid ratios.

The ^{1}H NOESY spectra of Antp(43−58) and Antp(43−58)-2F can be compared to spectra previously published for the MARCKS effector domain (*32*). The MARCKS(151−175) peptide is 25 residues in length and contains 13 basic amino acids and five phenylalanines. Electrostatic interactions mediate tight membrane binding (*37*), and the five aromatic residues penetrate into the hydrophobic core of the membrane (*32*, *35*). In fact, the aromatic rows of the ^{1}H NOESY spectrum obtained for MARCKS(151−175) bound to DMPC/DMPG multilayers are remarkably similar to those of Antp(43−58)-2F in Figures 2B and 4C. Together, these data indicate that basic−aromatic peptides with both helical and extended secondary structure penetrate the membrane surface to roughly the same extent. The only peptide that appears to penetrate the membrane more deeply is Antp(43−58), but only at a higher peptide concentration.

Finally, the Antp(43−58) peptide may be in equilibrium between deeply bound and surface-associated states. When the Antp(43−58) and Antp(43−58)-2F peptides are centrifuged in the presence of DMPC/DMPG vesicles at a peptide:lipid ratio of 4:100, most (>90%) of the Antp(43−58)-2F associates with the vesicles, whereas only approximately half of the Antp(43−58) peptide associates with the vesicles. Moreover, the Trp fluorescence studies showed that the Trp emission spectrum did not exhibit the blue shift expected for deeply buried Trp (*19*). In this regard, Nordén and coworkers have reported that Antp(43−58) induces vesicle aggregation followed by a spontaneous disaggregation (*31*). An equilibrium would be consistent with the NMR data presented above and with a dynamic process that allows the Antp(43−58) peptide to penetrate membranes.

^{31}P NMR of Bicelles and Multilayers. The ^{1}H NOESY data obtained using the Antp(43−58) peptide indicate that the peptide:lipid molar ratio influences the depth of peptide penetration. This suggests that there is an increase in the level of membrane disruption with an increase in peptide concentration, consistent with the observations of Binder and Lindbrom (*21*) and an electroporation-like mechanism for membrane penetration. To evaluate the effect of the Antp(43−58) and Antp(43−58)-2F peptides on membrane bilayer structure, ^{31}P NMR measurements were made as a function of the peptide concentration. ^{31}P NMR chemical shifts and line shapes are well-established tools for investigating changes in bilayer structure (*38*, *39*). Berlose et al. (*20*) have shown that binding of Antp(43−58) to membrane bilayers leads to a change in the isotropic and anisotropic contributions to the ^{31}P line shape. Our measurements extend these studies which were carried out for only a single concentration of Antp(43−58) and did not include the Antp(43−58)-2F peptide.

Figure 5 (left) presents ^{31}P spectra of oriented bicelles titrated with Antp(43−58) at peptide:lipid molar ratios from

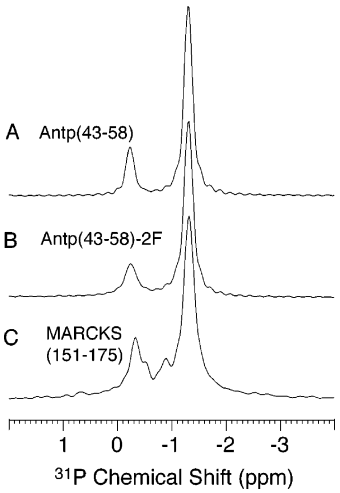

FIGURE 6: ^{31}P MAS spectra of Antp(43−58) (A) and Antp(43−58)-2F (B). The DMPC/DMPG/DHPC (10:3:3.25) bicelle samples with a peptide:lipid ratio of 4:100 were loaded into a 4 mm MAS rotor and spun at 6 kHz and 30 °C. MAS pellets the membrane lipids along the rotor walls. (C) ^{31}P MAS spectra of MARCKS-(151−175) at a peptide/lipid ratio of 4:100. ^{31}P chemical shifts were referenced to external 85% H_3PO_4.

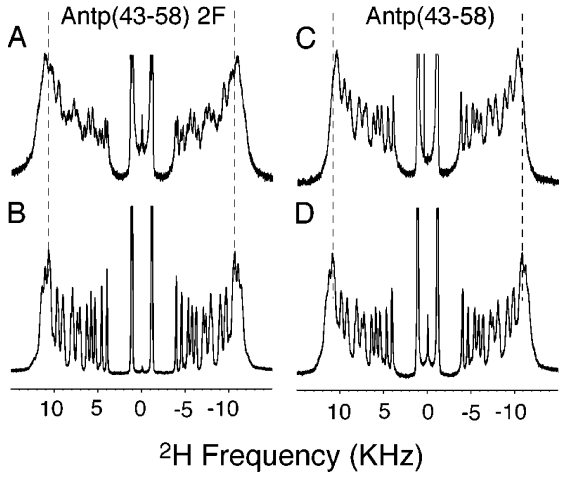

FIGURE 7: ^{2}H spectra of membrane bicelles containing Antp(43−58)-2F (A) and Antp(43−58) (C). The ^{2}H spectra were obtained with (A and C) and without (B and D) Antp peptide bound to oriented ($q = 4$) bicelles made from DMPC, DMPG, and DHPC (10:3:3.25) with a peptide/lipid ratio of 2:100. The DMPC is deuterated in both acyl chains.

0:100 to 4:100. In the oriented membrane bicelles, the ^{31}P spectrum is sensitive to the orientation of the phosphate headgroup. In bicelles without peptide, three distinct resonances are observed corresponding to the ^{31}P group of DMPC (−5.14 ppm), DMPG (−1.74 ppm), and DHPC (2.10 ppm). The large difference between DHPC and DMPC, both of which have PC headgroups, is due to the morphology of the $q = 4$ bicelles. The DMPC lipids are in the bilayer portion of the bicelle, and the lipid axis is roughly perpendicular to the *z*-axis of the magnetic field, whereas the DHPC lipids are on the edges of the bicelle roughly perpendicular to the DMPC lipids. DMPG is in the bilayer portion of the bicelle, but has a slightly different ^{31}P chemical shift due to a difference in the orientation of the headgroup. As Antp(43−58) is titrated into this system, the chemical shift of the DMPC resonance does not change. In contrast, the DMPG resonance changes from −1.74 to −0.27 ppm, moving closer to the resonance from DHPC.

Figure 5 (right) presents ^{31}P spectra of oriented bicelles titrated with Antp(43−58)-2F from a peptide:lipid molar ratio of 0:100 to a ratio of 4:100. The spectra are remarkably similar to those with Antp(43−58) in Figure 5 (left).

The dramatic shift of the ^{31}P resonance of DMPG upon addition of either Antp(43−58) or Antp(43−58)-2F can be caused by a change in the orientation of the DMPG headgroup or by a change in the local electrostatic environment. To address the origin of the shift, Figure 6 presents the ^{31}P MAS spectra of the membrane bicelles in Figure 5. The membrane lipids are no longer oriented in the MAS NMR rotor, and MAS yields only the isotropic component of the chemical shift tensor. The spectra show distinct resonances for DMPC/DHPC bilayers at −1.32 ppm and for DMPG at −0.33 ppm. There is no indication of a change in the ^{31}P chemical shift due to local electrostatic interactions. This argues that the DMPG shifts observed in Figure 5 are due to a change in DMPG orientation.

For comparison, Figure 6C presents the ^{31}P MAS spectrum of the MARCKS(151−175) effector domain. The positively charged amino acids in MARCKS(151−175) result in a change in the environment of the negatively charged phosphate headgroups and produce a unique set of chemical shifts.

^{2}H NMR of Bicelles and Multilayers. ^{2}H NMR is another method for characterizing bilayer structure. Bicelles enriched in DMPC with deuterated acyl chains were prepared by substituting 20% of the protonated DMPC normally present in the bicelles with chain deuterated DMPC. This level of deuteration was sufficient to obtain high-sensitivity spectra. The observed ^{2}H quadrupolar splitting (Δ) for lipid acyl chain deuterons in a bicelle depends on the quadrupolar coupling constant, e^2qQ/h, and the order parameter, S_{CD} (*40*, *41*). The quadrupolar coupling constant for an acyl chain C−D bond is ∼168 kHz. The observed quadrupolar splitting depends on the order parameter S_{CD}, which describes the orientation of the C−D bond vector relative to the external magnetic field and how that orientation is averaged by molecular motion. For membrane bicelles, changes in the order parameter (and the observed quadrupolar splitting) due to peptide binding can result from changes in the order or motion of the bicelle relative to the external magnetic field, changes in the motion of the individual phospholipids, and changes in the average orientation of individual C−D bonds relative to the molecular axis of the phospholipids (*40*).

Figure 7 presents deuterium NMR spectra of oriented bicelles with (A) and without (B) the addition of Antp(43−58)-2F. Oriented bicelles increase the spectral resolution for ^{2}H, making it an extremely sensitive probe of acyl chain orientation and motion (*42*). The C−D groups with the lowest order parameters correspond to the terminal methyl groups of the acyl chains and give rise to the intense resonances at ±1200 Hz. The resonances beyond ±10 kHz correspond to the methylene deuterons close to the acyl chain carbonyls. We observe a slight increase in the quadrupolar splitting with the addition of the Antp(43−58)-2F peptide (Figure 7A). This spectrum was obtained with a peptide: lipid molar ratio of 2:100, which corresponds to the midpoint of the titration in Figure 5. Of note is that the ^{31}P resonance of DMPC in Figure 5 (right) does not change in frequency or line width as Antp(43−58)-2F is titrated into the $q = 4$

bicelles. This suggests that the orientation or motion of the DMPC headgroup does not change when Antp(43−58)-2F binds to the bicelles. The bicelles appear to remain well-oriented. The increased quadrupolar splitting for the Antp-(43−58)-2F peptide is consistent with a decreased level of motion of the lipid acyl chains. We propose that this is due to insertion of the peptide into the acyl chain region of the bilayer as indicated by the ^{1}H NOESY measurements described above. We have recently observed a similar change in the quadrupolar splitting of deuterated $q = 4$ bicelles upon binding of the MARCKS(151−175) peptide (data not shown). In MARCKS(151−175), the five Phe residues insert through the polar headgroup region and pack against the acyl chains (*35*). The insertion of the Phe rings in both MARCKS-(151−175) and Antp(43−58)-2F results in a reduced level of lipid chain motion.

Figure 7 also presents deuterium NMR spectra of oriented bicelles with (C) and without (D) the addition of Antp(43−58). In contrast to that of Antp(43−58)-2F, binding of Antp-(43−58) results in a slight decrease in the quadrupolar splitting of all of the lipid acyl chain deuterons. Antp(43−58) binding also results in a slight broadening of the ^{31}P resonance of DMPC in $q = 4$ bicelles in Figure 5 (left). The decreased splitting for the Antp(43−58) peptide reflects the decreased average order of the lipid acyl chains, possibly due to local disruption of the bilayer.

Proposed Mechanism of Membrane Penetration of Antp-(43−58). The data obtained above allow us to distinguish between the three competing models for how Antp(43−58) crosses cell membranes. The ^{1}H NOESY data indicate that the peptides penetrate deeply into the bilayer and suggest that there is disruption of the local bilayer structure as the peptide concentration is increased. Deep penetration of aromatic residues has been shown in other systems (e.g., the MARCKS peptide) using both NMR (*32*, *43*) and EPR (*44*). This argues against the models based on endocytic pathways and the formation of inverse micelles where the peptides are thought to be associated with the bilayer surface.

Figure 8 presents a cartoon illustrating the initial steps involved in membrane penetration by Antp(43−58). Binding of the Antp(43−58) peptide to the hydrophilic region of the lipid headgroup is mediated by both the basic and aromatic amino acids. The aromatic amino acids then penetrate into the hydrocarbon interior of the membrane. Deep penetration of the peptide increases the electrostatic potential extending from the positively charged amino acids as they are pulled into a lower-dielectric environment (see refs *32* and *37*). The positive potential attracts negatively charged DMPG lipids. The model emphasizes that both electrostatic and hydrophobic interactions work in concert to mediate membrane penetration. Noncovalent cation−π interactions between the charged and hydrophobic side chains of arginine and tryptophan often occur in the membrane proteins (*45*). Such interactions may be occurring in Antp(43−58) to lower the energy cost of moving the positively charged arginine side chain into a lower-dielectric environment.

The shift in the ^{31}P resonance of DMPG in Figure 5 results from reorientation of the DMPG lipids adjacent to the peptide as it moves below the surface of the bilayer. This conclusion was confirmed by MAS NMR spectra of unoriented membranes. As the concentration of the peptide is increased, the orientation approaches that of DHPC which is perpendicular

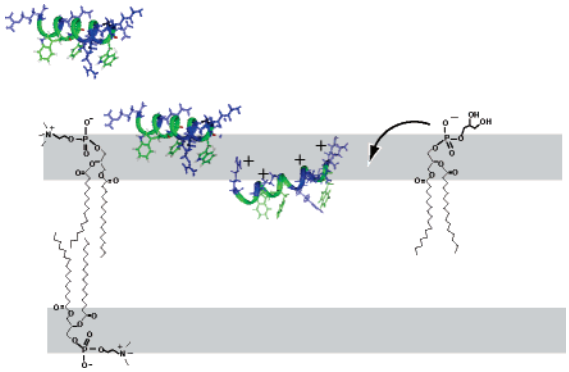

FIGURE 8: Model of binding of Antp(43−58) to membrane bilayers. The 16-residue Antp(43−58) peptide is helical in solution and binds to negatively charged membranes through electrostatic interactions of the six basic amino acids (colored blue) and hydrophobic interactions of the seven hydrophobic and aromatic amino acids (colored green). The side chains of the Trp residues penetrate to the level of the lipid acyl chains. The Antp(43−58) peptide is less helical at high peptide:lipid ratios (*16*, *17*), suggesting that in the membrane-spanning state the Antp(43−58) conformation is extended to allow the basic amino acids to reach the headgroup region of the bilayer. The ^{31}P NMR data indicate that the negatively charged DMPG lipids change orientation due to binding and penetration of the Antp(43−58) peptide.

to the bilayer surface. The concentration-dependent shift of the DMPG resonance indicates that Antp(43−58) peptides associate in a DMPG-rich region of the bilayer [i.e., the first Antp(43−58) peptide bound increases the local DMPG concentration, which then attracts additional Antp(43−58) peptides]. The observation that concentration-dependent ^{31}P chemical shifts occur in our membrane bicelle samples suggests that the peptides are preferentially binding to the same side of the bicelle as the peptide concentration is increased. The NOESY data for Antp(43−58) at a peptide:lipid molar ratio of 4:100 show that the Trp side chains penetrate to the level of the terminal methyl groups of the acyl chains. Deep penetration with an increased peptide concentration agrees well with the results of Binder and Lindblom (*21*), who found that at high peptide:lipid ratios (1:20) the asymmetric distribution of the positively charged peptide causes a transmembrane electric field. The local transmembrane electric field destabilizes the bilayer by increasing the lateral stress within the membrane (*21*).

The model that emerges from our studies is consistent with molecular dynamics simulations of pure phospholipid bilayers that capture the electroporation process (*46*) due to an applied external electric field. In these simulations, water defects that penetrate into the bilayer interior increase in likelihood with an increase in the applied electric field. This process initiates pore formation by allowing the phospholipids at the position of the defect to reorient and line the nascent pore. We suggest that the function of the Antp(43−58) peptide is to create high local electric field gradients at the site of peptide binding. With Antp(43−58), however, pores do not form.

The peptide may have an extended structure as it crosses the membrane. The Antp(43−58) peptide is helical at low peptide:lipid ratios and becomes less helical at high peptide:lipid ratios (*16*, *17*). Peptide permeation may be a transient event involving a single Antp(43−58) peptide whose N-terminal arginine crosses the hydrocarbon interior using local defects in the bilayer to remain hydrated. Our binding studies

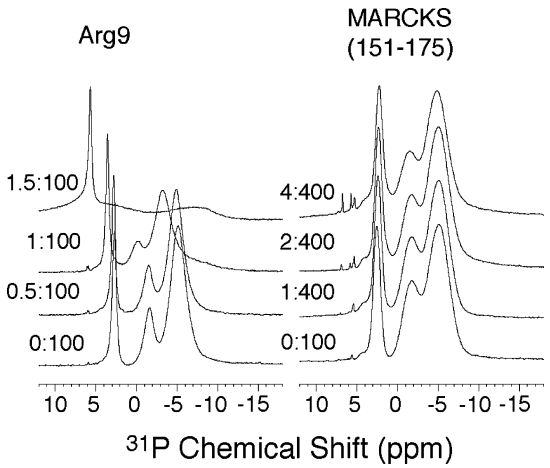

FIGURE 9: ^{31}P spectra of membrane bicelles containing Arg9 (left) and MARCKS(151−175) (right). The DMPC/DMPG/DHPC (10:3:3.25) bicelles were titrated with the Arg9 peptide at molar ratios (peptide:lipid) from 0:100 to 1.5:100, and with the MARCKS peptide at molar ratios (peptide:lipid) from 0:100 to 4:100. The temperature was maintained at 27 °C. ^{31}P chemical shifts were referenced to external 85% H_3PO_4.

on the Antp(43−58) peptide (data not shown) suggest that the peptide is in equilibrium between unbound and membrane-bound states. Alternatively, the association of Antp(43−58) with DMPG may form a transient structure involving several peptides and lipids. Molecular dynamics simulations and electrostatic calculations will be needed to evaluate these possibilities.

In conclusion, the NMR data presented above demonstrate the ability of the basic−aromatic motif of Antp(43−58) to mediate membrane binding and deep membrane penetration of the bilayer. The concentration-dependent change in the ^{31}P chemical shift of DMPG in the membrane bicelles is unusual. Neither Arg9 nor the MARCKS(151−178) peptide induces such changes (see Appendix). Further studies are in progress to establish the elements in the Antp(43−58) sequence that are responsible for this effect.

ACKNOWLEDGMENT

We gratefully acknowledge the W. M. Keck Foundation for support of the NMR facilities in the Center of Structural Biology at Stony Brook University. We thank Dr. Martine Ziliox for assistance with the NMR experiments and critical reading of the manuscript and Prof. Saburo Aimoto (Osaka University, Osaka, Japan) for peptide synthesis and purification.

APPENDIX

^{31}P NMR of Arg9 and MARCKS(151−175). The mechanism for how Antp(43−58) crosses cell membranes may be distinctly different from that of Arg9 and HIV-1 TAT, the peptides used by Melikov and colleagues (*23*) to assess the role of endocytosis. Arg9 has nine basic amino acids, and HIV-1 TAT has eight basic residues and a single N-terminal tyrosine.

For comparison with Antp(43−58), Figure 9 presents the ^{31}P spectra of oriented bicelles titrated with the nonapeptide Arg9 and the effector domain of the MARCKS protein. As Arg9 is titrated into the solution of bicelles, the DMPC and DMPG resonances broaden slightly up to a peptide:lipid molar ratio of 1:100 and then broaden dramatically at a molar ratio of 1.5:100. The DHPC resonance shifts from 2.7 to 5.6 ppm. At the 1.5:100 molar ratio, the chemical shift of the DHPC resonance (5.6 ppm) is the same as that obtained from pure DHPC micelles (data not shown). The positively charged Arg9 peptide appears to disrupt the bilayer structure of the bicelle at high peptide:lipid ratios. This is in distinct contrast to the behavior of Antp(43−58) and Antp(43−58)-2F, but agrees with studies showing that Arg9 induces leakage, but only at high peptide:lipid molar ratios (*24*).

The MARCKS(151−175) sequence has a relatively well characterized basic−aromatic motif. The MARCKS(151−175) peptide binds electrostatically to negatively charged membrane bilayers (*35*, *37*), and the five phenylalanines penetrate to the level of the lipid acyl chains (*32*, *35*). The peptide does not cross membrane bilayers, although the positive electrostatic potential recruits negatively charged lipids (*37*). Figure 9 presents ^{31}P NMR spectra of oriented bicelles titrated with MARCKS(151−175) at peptide:lipid molar ratios from 0:100 to 4:100. In bicelles without peptide, three distinct resonances are observed corresponding to the ^{31}P group of DMPC (−5.1 ppm), DMPG (−1.7 ppm), and DHPC (2.5 ppm). Unlike binding of Antp(43−58), binding of MARCKS(151−175) leads to the appearance of new resonances between 5 and 8 ppm. The main DMPG resonance at −1.7 ppm does not experience a change in frequency.

REFERENCES

1. McLaughlin, S., Wang, J. Y., Gambhir, A., and Murray, D. (2002) PIP2 and proteins: Interactions, organization, and information flow, *Annu. Rev. Biophys. Biomol. Struct. 31*, 151−175.
2. Derossi, D., Calvet, S., Trembleau, A., Brunissen, A., Chassaing, G., and Prochiantz, A. (1996) Cell internalization of the third helix of the antennapedia homeodomain is receptor-independent, *J. Biol. Chem. 271*, 18188−18193.
3. Prochiantz, A. (1999) Homeodomain-derived peptides: In and out of the cells, in *Anticancer Molecules: Structure, Function, and Design*, pp 172−179, New York Academy of Sciences, New York.
4. Schwarze, S. R., Hruska, K. A., and Dowdy, S. F. (2000) Protein transduction: Unrestricted delivery into all cells? *Trends Cell Biol. 10*, 290−295.
5. Curnow, P., Mellor, H., Stephens, D. J., Lorch, M., and Booth, P. J. (2005) Translocation of the cell-penetrating Tat peptide across artificial bilayers and into living cells, *Biochem. Soc. Symp. 72*, 199−209.
6. Oehlke, J., Birth, P., Klauschenz, E., Wiesner, B., Beyermann, M., Oksche, A., and Bienert, M. (2002) Cellular uptake of antisense oligonucleotides after complexing or conjugation with cell-penetrating model peptides, *Eur. J. Biochem. 269*, 4025−4032.
7. Schwartz, J. J., and Zhang, S. G. (2000) Peptide-mediated cellular delivery, *Curr. Opin. Mol. Ther. 2*, 162−167.
8. Derossi, D., Chassaing, G., and Prochiantz, A. (1998) Trojan peptides: The penetratin system for intracellular delivery, *Trends Cell Biol. 8*, 84−87.
9. Derossi, D., Joliot, A. H., Chassaing, G., and Prochiantz, A. (1994) The 3rd helix of the antennapedia homeodomain translocates through biological membranes, *J. Biol. Chem. 269*, 10444−10450.
10. Lindgren, M., Hallbrink, M., Prochiantz, A., and Langel, U. (2000) Cell-penetrating peptides, *Trends Pharmacol. Sci. 21*, 99−103.
11. Scheller, A., Oehlke, J., Wiesner, B., Dathe, M., Krause, E., Beyermann, M., Melzig, M., and Bienert, M. (1999) Structural requirements for cellular uptake of α-helical amphipathic peptides, *J. Pept. Sci. 5*, 185−194.
12. Drin, G., Mazel, M., Clair, P., Mathieu, D., Kaczorek, M., and Temsamani, J. (2001) Physico-chemical requirements for cellular uptake of pAntp peptide: Role of lipid-binding affinity, *Eur. J. Biochem. 268*, 1304−1314.

13. Drin, G., Demene, H., Temsamani, J., and Brasseur, R. (2001) Translocation of the pAntp peptide and its amphipathic analogue AP-2AL, *Biochemistry 40*, 1824−1834.
14. Williams, E. J., Dunican, D. J., Green, P. J., Howell, F. V., Derossi, D., Walsh, F. S., and Doherty, P. (1997) Selective inhibition of growth factor-stimulated mitogenesis by a cell-permeable Grb2-binding peptide, *J. Biol. Chem. 272*, 22349−22354.
15. Brugidou, J., Legrand, C., Mery, J., and Rabie, A. (1995) The retro-inverso form of a homeobox-derived short peptide is rapidly internalized by cultured neurons: A new basis for an efficient intracellular delivery system, *Biochem. Biophys. Res. Commun. 214*, 685−693.
16. Christiaens, B., Symoens, S., Vanderheyden, S., Engelborghs, Y., Joliot, A., Prochiantz, A., Vandekerckhove, J., Rosseneu, M., and Vanloo, B. (2002) Tryptophan fluorescence study of the interaction of penetratin peptides with model membranes, *Eur. J. Biochem. 269*, 2918−2926.
17. Christiaens, B., Grooten, J., Reusens, M., Joliot, A., Goethals, M., Vandekerckhove, J., Prochiantz, A., and Rosseneu, M. (2004) Membrane interaction and cellular internalization of penetratin peptides, *Eur. J. Biochem. 271*, 1187−1197.
18. Prochiantz, A. (1996) Getting hydrophilic compounds into cells: Lessons from homeopeptides. Commentary, *Curr. Opin. Neurobiol. 6*, 629−634.
19. Magzoub, M., Kirk, K., Eriksson, L. E. G., Langel, U., and Graslund, A. (2001) Interaction and structure induction of cell-penetrating peptides in the presence of phospholipid vesicles, *Biochim. Biophys. Acta 1512*, 77−89.
20. Berlose, J. P., Convert, O., Derossi, D., Brunissen, A., and Chassaing, G. (1996) Conformational and associative behaviours of the third helix of antennapedia homeodomain in membrane-mimetic environments, *Eur. J. Biochem. 242*, 372−386.
21. Binder, H., and Lindblom, G. (2003) Charge-dependent translocation of the Trojan peptide penetratin across lipid membranes, *Biophys. J. 85*, 982−995.
22. Lindberg, M., Biverstahl, H., Graslund, A., and Maler, L. (2003) Structure and positioning comparison of two variants of penetratin in two different membrane mimicking systems by NMR, *Eur. J. Biochem. 270*, 3055−3063.
23. Richard, J. P., Melikov, K., Vives, E., Ramos, C., Verbeure, B., Gait, M. J., Chernomordik, L. V., and Lebleu, B. (2003) Cell-penetrating peptides: A reevaluation of the mechanism of cellular uptake, *J. Biol. Chem. 278*, 585−590.
24. Fuchs, S. M., and Raines, R. T. (2004) Pathway for polyarginine entry into mammalian cells, *Biochemistry 43*, 2438−2444.
25. Chatelin, L., Volovitch, M., Joliot, A. H., Perez, F., and Prochiantz, A. (1996) Transcription factor Hoxa-5 is taken up by cells in culture and conveyed to their nuclei, *Mech. Dev. 55*, 111−117.
26. Perez, F., Lledo, P. M., Karagogeos, D., Vincent, J. D., Prochiantz, A., and Ayala, J. (1994) Rab3a and Rab3b carboxy-terminal peptides are both potent and specific inhibitors of prolactin-release by rat cultured anterior-pituitary-cells, *Mol. Endocrinol. 8*, 1278−1287.
27. Schwarze, S. R., Ho, A., Vocero-Akbani, A., and Dowdy, S. F. (1999) In vivo protein transduction: Delivery of a biologically active protein into the mouse, *Science 285*, 1569−1572.
28. Matsuzaki, K., Murase, O., Fujii, N., and Miyajima, K. (1995) Translocation of a channel-forming antimicrobial peptide, magainin-2, across lipid bilayers by forming a pore, *Biochemistry 34*, 6521−6526.
29. Matsuzaki, K., Yoneyama, S., Murase, O., and Miyajima, K. (1996) Transbilayer transport of ions and lipids coupled with mastoparan X translocation, *Biochemistry 35*, 8450−8456.
30. Matsuzaki, K., Yoneyama, S., and Miyajima, K. (1997) Pore formation and translocation of melittin, *Biophys. J. 73*, 831−838.
31. Persson, D., Thoren, P. E. G., Herner, M., Lincoln, P., and Norden, B. (2003) Application of a novel analysis to measure the binding of the membrane-translocating peptide penetratin to negatively charged liposomes, *Biochemistry 42*, 421−429.
32. Zhang, W., Crocker, E., McLaughlin, S., and Smith, S. O. (2003) Binding of peptides with basic and aromatic residues to bilayer membranes: Phenylalanine in the myristoylated alanine-rich C kinase substrate effector domain penetrates into the hydrophobic core of the bilayer, *J. Biol. Chem. 278*, 21459−21466.
33. Sanders, C. R., Hare, B. J., Howard, K., and Prestegard, J. H. (1994) Magnetically-oriented phospholipid micelles as a tool for the study of membrane-associated molecules, *Prog. Nucl. Magn. Reson. Spectrosc. 26*, 421−444.
34. van Dam, L., Karlsson, G., and Edwards, K. (2004) Direct observation and characterization of DMPC/DHPC aggregates under conditions relevant for biological solution NMR, *Biochim. Biophys. Acta 1664*, 241−256.
35. Ellena, J. F., Burnitz, M. C., and Cafiso, D. S. (2003) Location of the myristoylated alanine-rich C-kinase substrate (MARCKS) effector domain in negatively charged phospholipid bicelles, *Biophys. J. 85*, 2442−2448.
36. Huster, D., and Gawrisch, K. (1999) NOESY NMR crosspeaks between lipid headgroups and hydrocarbon chains: Spin diffusion or molecular disorder? *J. Am. Chem. Soc. 121*, 1992−1993.
37. Wang, J. Y., Gambhir, A., Hangyas-Mihalyne, G., Murray, D., Golebiewska, U., and McLaughlin, S. (2002) Lateral sequestration of phosphatidylinositol 4,5-bisphosphate by the basic effector domain of myristoylated alanine-rich C kinase substrate is due to nonspecific electrostatic interactions, *J. Biol. Chem. 277*, 34401−34412.
38. Tilcock, C. P. S., Cullis, P. R., and Gruner, S. M. (1986) On the validity of ^{31}P NMR determinations of phospholipid polymorphic phase-behavior, *Chem. Phys. Lipids 40*, 47−56.
39. Seelig, J. (1978) ^{31}P Nuclear magnetic resonance and head group structure of phospholipids in membranes, *Biochim. Biophys. Acta 515*, 105−140.
40. Prosser, R. S., Hwang, J. S., and Vold, R. R. (1998) Magnetically aligned phospholipid bilayers with positive ordering: A new model membrane system, *Biophys. J. 74*, 2405−2418.
41. Seelig, A., and Seelig, J. (1974) The dynamic structure of fatty acyl chains in a phospholipid bilayer measured by deuterium magnetic resonance, *Biochemistry 13*, 4839−4845.
42. Glover, K. J., Whiles, J. A., Wu, G. H., Yu, N. J., Deems, R., Struppe, J. O., Stark, R. E., Komives, E. A., and Vold, R. R. (2001) Structural evaluation of phospholipid bicelles for solution-state studies of membrane-associated biomolecules, *Biophys. J. 81*, 2163−2171.
43. Jing, W., Hunter, H. N., Hagel, J., and Vogel, H. J. (2003) The structure of the antimicrobial peptide Ac-RRWWRF-NH_2 bound to micelles and its interactions with phospholipid bilayers, *J. Pept. Res. 61*, 219−229.
44. Rauch, M. E., Ferguson, C. G., Prestwich, G. D., and Cafiso, D. S. (2002) Myristoylated alanine-rich C kinase substrate (MARCKS) sequesters spin-labeled phosphatidylinositol 4,5-bisphosphate in lipid bilayers, *J. Biol. Chem. 277*, 14068−14076.
45. Gromiha, M. M., and Suwa, M. (2005) Structural analysis of residues involving cation-π interactions in different folding types of membrane proteins, *Int. J. Biol. Macromol. 35*, 55−62.
46. Tieleman, D. P. (2004) The molecular basis of electroporation, *BMC Biochem. 5*, 10−21.

BI050341V